Temperature-dependent cross sections for meson-meson nonresonant reactions in hadronic matter

Yi-Ping Zhang Xiao-Ming Xu Hui-Jun Ge

Department of Physics, Shanghai University, Baoshan, Shanghai 200444, China

Abstract

We present a potential of which the short-distance part is given by one gluon exchange plus perturbative one- and two-loop corrections and of which the large-distance part exhibits a temperature-dependent constant value. The Schrödinger equation with this temperature-dependent potential yields a temperature dependence of the mesonic quark-antiquark relative-motion wave function and of meson masses. The temperature dependence of the potential, the wave function and the meson masses brings about temperature dependence of cross sections for the nonresonant reactions $\pi\pi \to \rho\rho$ for $I = 2$, $KK \to K^*K^*$ for $I = 1$, $KK^* \to K^*K^*$ for $I = 1$, $\pi K \to \rho K^*$ for $I = 3/2$, $\pi K^* \to \rho K^*$ for $I = 3/2$, $\rho K \to \rho K^*$ for $I = 3/2$ and $\pi K^* \to \rho K$ for $I = 3/2$. As the temperature increases, the rise or fall of peak cross sections is determined by the increased radii of initial mesons, the loosened bound states of final mesons, and the total-mass difference of the initial and final mesons. The temperature-dependent cross sections and meson masses are parametrized.

PACS: 25.75.-q; 13.75.Lb; 12.38.Mh

Keywords: Meson-meson nonresonant reaction; Cross section; Quark-interchange mechanism.

1. Introduction

In spite of scarce experimental data of cross sections for inelastic meson-meson scattering, these cross sections can be calculated from quark potential models, parton distributions or effective meson Lagrangians that respect various symmetries. This has been seen from the dissociation cross sections of J/ψ in collisions with mesons, which have received much attention. For example, cross sections for reactions like $\pi + J/\psi \to D\bar{D}^* + D^*\bar{D} + D^*\bar{D}^*$ and $\rho + J/\psi \to D\bar{D}^* + D^*\bar{D} + D^*\bar{D}^*$ were obtained with the quark-interchange mechanism [1,2] in different quark potential models [3–6]. The quark-interchange models give the characteristic that cross sections for endothermic reactions first increase from threshold energies and then decrease as the center-of-mass energy of J/ψ and hadron increases. A very small low-energy nucleon-J/ψ break-up cross section was obtained by using the operator product expansion for the elastic scattering amplitude of J/ψ [7–9]. The dissociation cross section for $\pi - J/\psi$, evaluated in QCD sum rules [10] in the soft-pion limit, increases gradually in contrast to rapid growth near the threshold energy obtained in meson exchange [11–15] and quark interchange models [3–6].

In comparison to meson-J/ψ reactions, however, cross sections for inelastic scattering of a light meson by another light meson are rarely studied. Inelastic scattering between light mesons does occur in hadronic matter and the cross sections involved influence the time dependence of meson momentum distributions and flavor dependence of the measured momentum distributions at kinetic freeze-out. In order to understand this influence, the cross sections for inelastic scattering and their relevant characteristics must be studied. Since hadronic matter produced in Au-Au collisions at the Relativistic Heavy Ion Collider mainly consists of pions, rhos and kaons [16–23], in this work we pay attention only to the nonresonant reactions of the four mesons π, ρ, K and K^*, which are taken to be governed by quark-interchange processes. In Ref. [24] we have calculated in-vacuum cross sections for the nonresonant reactions $\pi\pi \to \rho\rho$ for $I = 2$, $KK \to K^*K^*$ for $I = 1$, $KK^* \to K^*K^*$ for $I = 1$, $\pi K \to \rho K^*$ for $I = 3/2$, $\pi K^* \to \rho K^*$ for $I = 3/2$, $\rho K \to \rho K^*$ for $I = 3/2$ and $\pi K^* \to \rho K$ for $I = 3/2$. The cross sections for the seven endothermic reactions depend

on the center-of-mass energy $\sqrt{s}$ of the two initial mesons and the energy where the maximum of cross section occurs is mainly determined by the maximum of $\mid \vec{P}' \mid / s \mid \vec{P} \mid$, where $\vec{P}$ and $\vec{P}'$ are the momenta of the initial and final mesons in the center-of-mass frame, respectively. The endothermic reactions have maximum cross sections ranging from 0.47 mb to 1.41 mb. These cross sections are obtained with a quark-quark potential that includes the linear confinement and one-gluon-exchange potential plus perturbative one- and two-loop corrections [6]. At nonzero temperature the linear confinement is modified to become weaker. At a temperature below the critical temperature T_c of the QCD phase transition, medium effects show up in the region where the quark-antiquark distance is larger than 0.3 fm [25]. When the quark-antiquark distance is large enough, the quark-antiquark potential at a given temperature becomes constant. This temperature-dependent potential must change the wave function of quark-antiquark relative motion in a meson and cross sections for inelastic meson-meson scattering are expected to change with temperature as well. Therefore, in this work we study the dependence of cross sections on the temperature for the nonresonant reactions $\pi\pi \to \rho\rho$ for $I = 2$, $KK \to K^*K^*$ for $I = 1$, $KK^* \to K^*K^*$ for $I = 1$, $\pi K \to \rho K^*$ for $I = 3/2$, $\pi K^* \to \rho K^*$ for $I = 3/2$, $\rho K \to \rho K^*$ for $I = 3/2$ and $\pi K^* \to \rho K$ for $I = 3/2$. Until now the temperature dependence of the cross sections has not been studied in experiments or theory.

In the next section, we present a potential of which the short-distance part is given by perturbative QCD and the large-distance part is displayed in the lattice gauge results of Ref. [25]. The Schrödinger equation with the potential is solved to get the quark-antiquark relative-motion wave function of a meson. A convenient framework for application of the temperature-dependent potential to inelastic meson-meson scattering is the Born approximation for the quark-interchange processes. In Section 3 we review formulas of cross sections for meson-meson nonresonant reactions that are based on the Born approximation. In Section 4 we show numerical results of cross sections and give relevant discussions. Parametrizations of the cross sections are given. Conclusions are in the last section.

2. Potential and wave functions of quark-antiquark relative motion

In Ref. [25] the heavy quark potential was assumed to be equal to the free energy of heavy quark-antiquark pair and the lattice calculations provided the temperature dependence of the potential. When the distance r between quark and antiquark is large enough, the potential at a given temperature exhibits a constant value and becomes a plateau. This value depends on the temperature T and decreases with increasing temperature. The constant value at large distances can be parametrized as

$$V_{ab}(\vec{r}) = -\frac{\vec{\lambda}_a}{2} \cdot \frac{\vec{\lambda}_b}{2} \frac{3}{4} D \left[1.3 - \left(\frac{T}{T_c} \right)^4 \right], \tag{1}$$

with $D = 0.7$ GeV and $T_c = 0.175$ GeV. Here $\vec{\lambda}$ are the Gell-Mann matrices for the color generators. D is a fit parameter, but happens to equal the height of the plateau of $T = 0.74 T_c$.

The relative color orientation of two constituents (quarks and antiquarks here) can be indicated by wave functions of the two constituents. The expectation value of $\frac{\vec{\lambda}_a}{2} \cdot \frac{\vec{\lambda}_b}{2}$ depends on the relative color orientation, so does the heavy quark potential given in Eq. (1). The dependence of the potential on the relative color orientation is supported by hadronic physics and lattice calculations. We discuss evidence in the three cases: (a) $T = 0$, (b) $T > T_c$ and (c) $0 < T < T_c$.

(a) Since the establishment of QCD the dependence of confinement with $\frac{\vec{\lambda}_a}{2} \cdot \frac{\vec{\lambda}_b}{2}$ on the relative color orientation has been widely used in hadronic physics, for instance, meson-baryon scattering [26] and meson-meson scattering [5]. The expectation value of $\frac{\vec{\lambda}_a}{2} \cdot \frac{\vec{\lambda}_b}{2}$ is negative in the color singlet state and positive in any color octet state. This complies with the fact that the color singlet state is observed and the color octet states are not observed.

(b) When temperature is above T_c, it is expected in Ref. [27] that the interaction in an antitriplet diquark system is only half as strong as in a color-singlet quark-antiquark system, i.e. obeys Casimir scaling, and the interaction depends on the relative color orientation.

(c) When temperature is between 0 and T_c, the situation is complicated. From Figs. 15, 17 and 20 in Ref. [28], we can derive that the color-singlet free energy does not equal

the color-octet free energy at large distances in the region $0.907T_c \leq T < T_c$. It can also be expected from Fig. 3 of Ref. [27] that the interaction in an antitriplet diquark system is nearly half as strong as in a color-singlet quark-antiquark system, i.e. the interaction depends on the relative color orientation in the region $0.87T_c \leq T < T_c$.

Much attention has been paid to construction of the color octet potential from perturbative QCD and lattice data in the study of hybrid mesons. The color octet potential relies on the spatial extension of gluon field confined in hybrid mesons. In the string description the symmetry of the gluon field is labeled by the spins Σ, Π and Δ about the axis connecting the quark and antiquark, a PC value and an additional reflection symmetry for Σ states. It was obtained in vacuum that the color octet potential is different with respect to different symmetries of the gluon field [29, 30]. Temperature dependence of the gluon field affects temperature dependence of the color octet potential. How does the gluon field confined in a meson depend on temperature at $0 < T < T_c$? This is a difficult problem.

In summary, we still lack of the lattice study of the color octet potential at $0 < T < T_c$ and the heavy quark potential depends on the relative color orientation.

The large-distance plateau of the heavy quark potential indicates the onset of string breaking at a certain distance [27]. The string breaking occurs when the energy stored in the string exceeds the mass of a light quark-antiquark pair [31]. The combination of the light quark and the heavy antiquark and the combination of the light antiquark and the heavy quark form open heavy flavors. When the temperature is higher, light mesons in medium more effectively take a kind of flip-flop recoupling of quark constituents [32–34] and string breaking occurs at a shorter distance. Hence, the plateau appears at a shorter distance and confinement gets weaker. Consequently, the wave function of the heavy quark-antiquark pair becomes wider in space.

However, uncertainty of the heavy quark potential exists because the potential is derived from Polyakov loop correlation functions. The Polyakov loop at the space coordinate $\vec{r}_1$ is indicated by $L(\vec{r}_1)$. The Polyakov loop correlation functions are related to the free

energy of heavy quark-antiquark pair $F(T,r)$

$$-T\ln < L(\vec{r}_1)L^+(\vec{r}_2) >= F(T,r) + C \tag{2}$$

where $r =\mid \vec{r}_1 - \vec{r}_2 \mid$ and C is a normalization constant. The free energy leads to the internal energy by

$$U(T,r) = F(T,r) + TS(T,r) \tag{3}$$

The entropy $S(T,r) = -\partial F(T,r)/\partial T$ is independent of r at large distances and depends on r at the other distances. If TS is small, $U(T,r) \approx F(T,r)$; otherwise, the internal energy deviates from the free energy. Taking the free energy as the heavy quark potential like Ref. [25] is an approximation. Then the internal energy was suggested in Refs. [35,36] as the heavy quark potential. Very recently the heavy quark potential is argued to be the internal energy which is the expectation value of the difference of the Hamiltonians with and without the heavy quark-antiquark pair at rest [37,38], and this results in dissociation temperatures of heavy quarkonia that agree quite well with the values from lattice studies.

How to find the correct heavy quark potential is an important problem but has not been solved so far. It has been proposed that the heavy quark potential takes the form $\xi U(T,r) + (1-\xi)F(T,r)$ where the quantity ξ is between 0 and 1 and was determined in models [39–45]. Since the present lattice calculations provide the internal energy U that includes the internal energy of the heavy quark-antiquark pair and the gluon internal energy difference $U_{\rm g}(T,r) - U_{\rm g0}(T)$ where $U_{\rm g}(T,r)$ and $U_{\rm g0}(T)$ correspond to the gluon internal energies in the presence and absence of the heavy quark-antiquark pair, respectively, it was proposed by Wong [41] that the heavy quark potential should be $U(T,r) - [U_{\rm g}(T,r) - U_{\rm g0}(T)]$. In the local energy-density approximation that adopts an equation of state for the quark-gluon plasma, the heavy quark potential can be represented as a linear combination of F and U. With F and U obtained in lattice calculations in quenched QCD, the potential gives spontaneous dissociation temperatures of heavy quarkonia that agree with those obtained from spectral analyses in quenched QCD [43]. This is an improvement in comparison to the use of F as a potential. The work of Wong implies that the heavy quark potential properly defined gives reliable results. Even though

the method of Wong has not been applied to hadronic matter, we still expect that the heavy quark potential for hadronic matter, if obtained, can produce more reliable cross sections for the meson-meson nonresonant reactions in the nonzero temperature region of hadronic matter than those from F.

At very small distances $r < 0.01$ fm, the potential obtained from one-gluon exchange plus one- and two-loop corrections in perturbative QCD is [46]

$$V_{ab}(\vec{r}) = \frac{\vec{\lambda}_a}{2} \cdot \frac{\vec{\lambda}_b}{2} \frac{12\pi}{25rw} \left[1 + \left(2\gamma_E + \frac{53}{75} \right) \frac{1}{w} - \frac{462}{625} \frac{\ln w}{w} \right], \tag{4}$$

where γ_E is the Euler's constant and $w = \ln(1/\Lambda^2_{\overline{\rm MS}} r^2)$ with the QCD scale parameter $\Lambda_{\overline{\rm MS}}$ determined by Eq. (2.13) in Ref. [46].

An interpolation between the constant confinement at large distances given in Eq. (1) and the spin-independent perturbative potential given in Eq. (4) produces a central spin-independent potential

$$V_{ab}(\vec{r}) = -\frac{\vec{\lambda}_a}{2} \cdot \frac{\vec{\lambda}_b}{2} \frac{3}{4} D \left[1.3 - \left(\frac{T}{T_c} \right)^4 \right] \tanh(Ar) + \frac{\vec{\lambda}_a}{2} \cdot \frac{\vec{\lambda}_b}{2} \frac{6\pi}{25} \frac{v(\lambda r)}{r} \exp(-Er), \tag{5}$$

where

$$A = 1.5[0.75 + 0.25(\frac{T}{T_c})^{10}]^6 \text{ GeV}, \tag{6}$$

and

$$E = 0.6 \text{ GeV}, \tag{7}$$

are fit parameters, and

$$\lambda = \sqrt{3b_0/16\pi^2\alpha'}, \tag{8}$$

$\alpha' = 1.04$ GeV^{-2} is the Regge slope and $b_0 = 11 - \frac{2}{3}N_f$ with the quark flavor number $N_f = 4$ [46]. This potential is different from the parametrizations given by Digal et al. [39] and Wong [47]. The potential contains the dimensionless function [46]

$$v(x) = \frac{4b_0}{\pi} \int_0^\infty \frac{dQ}{Q} (\rho(\vec{Q}^2) - \frac{K}{\vec{Q}^2}) \sin(\frac{Q}{\lambda} x), \tag{9}$$

with $K = 3/16\pi^2\alpha'$, where Q is the absolute value of gluon momentum $\vec{Q}$ and $\rho(\vec{Q}^2)$ is given by Buchmüller and Tye [46]. The quantity $\rho - \frac{K}{\vec{Q}^2}$ arises from one-gluon exchange and

perturbative one- and two-loop corrections. $\exp(-Er)$ is a medium modification factor to the potential of one-gluon exchange plus perturbative one- and two-loop corrections. The temperature correction to the one-gluon-exchange potential with the limit shown in Eq. (4) is the difference between the second term in Eq. (5) and the perturbative potential $\frac{\vec{\lambda}_a}{2} \cdot \frac{\vec{\lambda}_b}{2} \frac{6\pi}{25} \frac{v(\lambda r)}{r}$ [46]. The temperature correction is completely negligible at very short distances and obvious at intermediate and large distances.

The parametrization in Eq. (5) versus lattice gauge results is plotted in Fig. 1. It is clearly seen that a lower plateau at large distances corresponds to a higher temperature. Plateaus at $T/T_c = 0.97$, 0.94, 0.9, 0.84 approximately begin at $r = 1.15$ fm, 1.18 fm, 1.26 fm, 1.38 fm, respectively. Hence, a higher plateau begins at a larger distance. Confinement can be assumed to be flavor-independent in hadronic physics. For example, it was shown in Refs. [48–53] that quark-quark potentials with flavor-independent confinement, a Coulomb term and hyperfine interactions can consistently describe a large body of data like masses from light to heavy hadrons. The light hadrons may consist of only up and down quarks and the heavy hadrons may contain charm and bottom quarks. The flavor dependence of the quark-quark potentials is relevant to quark masses in the hyperfine interactions. The success of the potentials renders that the flavor independence of confinement is universal and the hyperfine interactions must be flavor-dependent. Therefore, the potential in Eq. (5) is reasonably flavor-independent. The potential obtained by Karsch et al. for heavy quarks is applied to light quarks. It is shown by the lattice calculations that screening sets in at distances $r \approx 0.3$ fm. However, present lattice calculations at finite temperatures are probably not yet precise enough to reach sufficiently short distances. Hence, a lattice-based potential has a degree of freedom in choosing its form at short distances. We construct the potential in Eq. (5) from the fact that the quark-quark interaction at $r < 0.01$ fm originates from one-gluon exchange plus loop corrections in perturbative QCD. The degree of freedom is removed at $r < 0.01$ fm.

The medium screening obtained in the lattice gauge calculations at present affects only the central spin-independent potential. This allows us to keep using the spin-spin interaction relevant to perturbative QCD, as done by Wong [47]. In our work, the spin-

spin interaction arises not only from one-gluon exchange but also from perturbative one- and two-loop corrections [6]

$$V_{\rm ss} = -\frac{\vec{\lambda}_a}{2}\cdot\frac{\vec{\lambda}_b}{2}\frac{16\pi^2}{25}\delta^3(\vec{r})\frac{\vec{s}_a\cdot\vec{s}_b}{m_a m_b} + \frac{\vec{\lambda}_a}{2}\cdot\frac{\vec{\lambda}_b}{2}\frac{4\pi}{25}\frac{1}{r}\frac{d^2v(\lambda r)}{dr^2}\frac{\vec{s}_a\cdot\vec{s}_b}{m_a m_b}, \tag{10}$$

where $\vec{s}_a$ and m_a are the spin and mass of constituent quarks or antiquarks labeled as a, respectively. This expression of the spin-spin interaction comes from the application of Eq. (7e) in the transformed Hamiltonian obtained by Chraplyvy [54] from the two-constituent Hamiltonian that includes the relativistic potential originating from one-gluon exchange plus perturbative one- and two-loop corrections [6]. The transformed Hamiltonian was obtained from an application of the Foldy-Wouthuysen canonical transformation to a relativistic two-particle Hamiltonian. The spin-spin interaction is related to the terms of the direct product of two Dirac α matrices [55] in the relativistic potential.

Given the masses $m_{\rm u} = m_{\rm d} = 0.32$ GeV for the up and down quarks, the Schrödinger equation with the central spin-independent potential in Eq. (5) is solved at $T = 0$ to obtain a radial wave function $R_{q\bar{q}}(T = 0, r)$ for the quark-antiquark relative motion of π and ρ mesons. Assuming all the mesons in the ground-state pseudoscalar octet and the ground-state vector nonet taking the same spatial wave function of quark-antiquark relative motion as the π and ρ mesons, the spin-spin interaction leads to the mass splitting between a pseudoscalar meson and a vector meson with the same isospin quantum number

$$< V_{\rm ss} >= \frac{16\pi}{75 m_a m_b}[R^2_{q\bar{q}}(T = 0, r = 0) - \int_0^\infty dr r \frac{d^2v(\lambda r)}{dr^2} R^2_{q\bar{q}}(T = 0, r)], \tag{11}$$

where $R_{q\bar{q}}$ satisfies the normalization condition $\int_0^\infty dr r^2 R^2_{q\bar{q}}(T, r) = 1$. At $m_{\rm s} = 0.5$ GeV for the strange-quark mass, the spin-spin interaction yields the mass splittings $m_\rho - m_\pi = 0.5989$ GeV, $m_{K^*} - m_K = 0.3833$ GeV and $\frac{1}{3}m_\omega + \frac{2}{3}m_\phi - m_\eta = 0.3622$ GeV, where m_i ($i = \pi, \rho, K, K^*, \eta, \omega, \phi$) represent the masses of $\pi, \rho, K, K^*, \eta, \omega$ and ϕ, respectively. These mass splittings can be compared to the experimental values 0.6304 GeV, 0.3963 GeV and 0.3930 GeV, respectively.

The spin-averaged mass of a spin-0 meson and a spin-1 meson with the same isospin is one-fourth of the spin-0 meson mass plus three-fourths of the spin-1 meson mass [3]. In

Table 1 we list vacuum masses of π, ρ, K and K^*, the spin-averaged mass $\overline{m}_{\pi\rho}$ of π and ρ and the one $\overline{m}_{KK^*}$ of K and K^*. The theoretical values of $\overline{m}_{\pi\rho}$, $\overline{m}_{KK^*}$, m_ρ, m_K and m_{K^*} approach the corresponding experimental data. The pion mass from our calculations almost doubles the experimental value. These are understandable. The potential given in Eq. (5) has the behavior of $\tanh(Ar)$ at large distances and cannot mimic the linear confinement. In vacuum the pion with the lightest mass among mesons has the largest radius and is sensitive to the potential behavior at large distances. Therefore, the experimental datum of pion mass must differ from the value derived from the potential. For ρ, K and K^* with masses larger than π, less sensitivity to the potential behavior at large distances does not lead to a large separation of the experimental and theoretical masses. If the theoretical pion mass is used, cross sections for pions in collisions with mesons are not reliable. Hence, the experimental values of meson masses are used in calculating meson-meson cross sections at $T = 0$ GeV in this work and, as will see, the cross sections are similar to those obtained from the potential with the linear confinement in Ref. [24].

If the quark masses are set equal to zero, the QCD Hamiltonian is symmetric under the chiral group $SU(3) \times SU(3)$. Although the spontaneous breakdown of the chiral symmetry is widely expected, the problem of calculating the spontaneous chiral symmetry breaking in QCD has not yet been satisfactorily solved [56,57]. However, the spontaneous symmetry breaking can be related to the quark condensate which vanishes in perturbative QCD and does not equal zero in the non-perturbative region. With the explicit breakdown of the chiral symmetry due to the current quark masses, the square of pion mass is proportional to the product of the quark condensate and the sum of the up and down quark masses at the lowest order in chiral perturbation theory. Therefore, the small pion mass comes from the small quark masses and the non-vanishing quark condensate in the non-perturbative region where confinement sets in. While only the spontaneous symmetry breaking occurs, Goldstone bosons and quarks are massless and the soft-pion theorems obtained in the vanishing pion four-momentum are exact [58]. While the explicit chiral symmetry breaking also occurs, bosons get masses and the soft-pion theorems become approximate. The deviation of the theorems from the experimental data has been studied

in chiral perturbation theory and the soft-pion theorems have been corrected [59–62]. In our work all the mesons in the ground-state pseudoscalar octet and the ground-state vector nonet are assumed to take the same spatial wave function of quark-antiquark relative motion as the pion and rho mesons, but the quark masses are the constituent masses which are much larger than the current quark masses used in chiral perturbation theory. The constituent quark masses show the explicit chiral symmetry breaking so that mesons get masses and the soft-pion theorems are violated. The cross sections that we will obtain from the constituent quark masses and the nonzero meson masses must deviate from the cross sections obtained from vanishing masses of quarks and mesons. Therefore, the deviation of our results from the soft-pion theorems should be expected.

3. Formulas for cross sections

Let m_i and $P_i = (E_i, \vec{P}_i)$ be the mass and the four-momentum of meson i ($i = q_1\bar{q}_1, q_2\bar{q}_2, q_1\bar{q}_2, q_2\bar{q}_1$), respectively. The Mandelstam variables for the reaction $A(q_1\overline{q}_1) + B(q_2\overline{q}_2) \to C(q_1\overline{q}_2) + D(q_2\overline{q}_1)$ are $s = (E_{q_1\bar{q}_1} + E_{q_2\bar{q}_2})^2 - (\vec{P}_{q_1\bar{q}_1} + \vec{P}_{q_2\bar{q}_2})^2$ and $t = (E_{q_1\bar{q}_1} - E_{q_1\bar{q}_2})^2 - (\vec{P}_{q_1\bar{q}_1} - \vec{P}_{q_1\bar{q}_2})^2$. In the center-of-mass frame the meson $A(q_1\overline{q}_1)$ has the momentum $\vec{P} = \vec{P}_{q_1\bar{q}_1} = -\vec{P}_{q_2\bar{q}_2}$ and the meson $C(q_1\overline{q}_2)$ has the momentum $\vec{P}' = \vec{P}_{q_1\bar{q}_2} = -\vec{P}_{q_2\bar{q}_1}$. $\vec{P}$ and $\vec{P}'$ are expressed in terms of s by

$$|\vec{P}(\sqrt{s})|^2 = \frac{1}{4s}\left\{\left[s - \left(m^2_{q_1\bar{q}_1} + m^2_{q_2\bar{q}_2}\right)\right]^2 - 4m^2_{q_1\bar{q}_1}m^2_{q_2\bar{q}_2}\right\}, \tag{12}$$

$$|\vec{P}'(\sqrt{s})|^2 = \frac{1}{4s}\left\{\left[s - \left(m^2_{q_1\bar{q}_2} + m^2_{q_2\bar{q}_1}\right)\right]^2 - 4m^2_{q_1\bar{q}_2}m^2_{q_2\bar{q}_1}\right\}. \tag{13}$$

Denote the angle between $\vec{P}$ and $\vec{P}'$ by θ. The cross section for $A(q_1\overline{q}_1) + B(q_2\overline{q}_2) \to C(q_1\overline{q}_2) + D(q_2\overline{q}_1)$ is

$$\sigma = \frac{1}{32\pi s}\frac{|\vec{P}'(\sqrt{s})|}{|\vec{P}(\sqrt{s})|}\int_0^\pi d\theta |\mathcal{M}_{\rm fi}(s,t)|^2 \sin\theta. \tag{14}$$

This formula provides the dependence on the total energy $\sqrt{s}$ of the two initial mesons in the center-of-mass frame and is valid for the interchange of the two quarks (q_1 and q_2) or of the two antiquarks ($\bar{q}_1$ and $\bar{q}_2$). The interchange of quarks brings about two forms of scattering that may lead to different values of the transition amplitude $\mathcal{M}_{\rm fi}$. The

forms are known as the prior form and the post form [63–65]. Scattering in the prior form means that gluon exchange takes place prior to the quark or antiquark interchange. The transition amplitude in the prior form is [24]

$$\begin{aligned}\mathcal{M}_{\rm fi}^{\rm prior} &= \sqrt{2E_{q_1\bar{q}_1}2E_{q_2\bar{q}_2}2E_{q_1\bar{q}_2}2E_{q_2\bar{q}_1}}\int\frac{d^3p_{q_1\bar{q}_2}}{(2\pi)^3}\frac{d^3p_{q_2\bar{q}_1}}{(2\pi)^3}\\ &\psi^+_{q_1\bar{q}_2}(\vec{p}_{q_1\bar{q}_2})\psi^+_{q_2\bar{q}_1}(\vec{p}_{q_2\bar{q}_1})(V_{q_1\bar{q}_2}+V_{\bar{q}_1q_2}+V_{q_1q_2}+V_{\bar{q}_1\bar{q}_2})\psi_{q_1\bar{q}_1}(\vec{p}_{q_1\bar{q}_1})\psi_{q_2\bar{q}_2}(\vec{p}_{q_2\bar{q}_2}),\end{aligned} \tag{15}$$

where $\psi_{ab}(\vec{p}_{ab})$ is the product of color, spin, flavor and momentum-space wave functions of the relative motion of constituents a and b and satisfies $\int\frac{d^3p_{ab}}{(2\pi)^3}\psi^+_{ab}(\vec{p}_{ab})\psi_{ab}(\vec{p}_{ab})=1$. The relative momentum of a and b is $\vec{p}_{ab}$. Scattering in the post form means that the quark or antiquark interchange is followed by gluon exchange. The transition amplitude in the post form is [24]

$$\begin{aligned}\mathcal{M}_{\rm fi}^{\rm post} &= \sqrt{2E_{q_1\bar{q}_1}2E_{q_2\bar{q}_2}2E_{q_1\bar{q}_2}2E_{q_2\bar{q}_1}}\\ &\left(\int\frac{d^3p_{q_1\bar{q}_1}}{(2\pi)^3}\frac{d^3p_{q_1\bar{q}_2}}{(2\pi)^3}\psi^+_{q_1\bar{q}_2}(\vec{p}_{q_1\bar{q}_2})\psi^+_{q_2\bar{q}_1}(\vec{p}_{q_2\bar{q}_1})V_{q_1\bar{q}_1}\psi_{q_1\bar{q}_1}(\vec{p}_{q_1\bar{q}_1})\psi_{q_2\bar{q}_2}(\vec{p}_{q_2\bar{q}_2})\right.\\ &+\int\frac{d^3p_{q_2\bar{q}_2}}{(2\pi)^3}\frac{d^3p_{q_2\bar{q}_1}}{(2\pi)^3}\psi^+_{q_1\bar{q}_2}(\vec{p}_{q_1\bar{q}_2})\psi^+_{q_2\bar{q}_1}(\vec{p}_{q_2\bar{q}_1})V_{\bar{q}_2q_2}\psi_{q_1\bar{q}_1}(\vec{p}_{q_1\bar{q}_1})\psi_{q_2\bar{q}_2}(\vec{p}_{q_2\bar{q}_2})\\ &+\int\frac{d^3p_{q_1\bar{q}_2}}{(2\pi)^3}\frac{d^3p_{q_2\bar{q}_1}}{(2\pi)^3}\psi^+_{q_1\bar{q}_2}(\vec{p}_{q_1\bar{q}_2})\psi^+_{q_2\bar{q}_1}(\vec{p}_{q_2\bar{q}_1})V_{q_1q_2}\psi_{q_1\bar{q}_1}(\vec{p}_{q_1\bar{q}_1})\psi_{q_2\bar{q}_2}(\vec{p}_{q_2\bar{q}_2})\\ &\left.+\int\frac{d^3p_{q_1\bar{q}_2}}{(2\pi)^3}\frac{d^3p_{q_2\bar{q}_1}}{(2\pi)^3}\psi^+_{q_1\bar{q}_2}(\vec{p}_{q_1\bar{q}_2})\psi^+_{q_2\bar{q}_1}(\vec{p}_{q_2\bar{q}_1})V_{\bar{q}_1\bar{q}_2}\psi_{q_1\bar{q}_1}(\vec{p}_{q_1\bar{q}_1})\psi_{q_2\bar{q}_2}(\vec{p}_{q_2\bar{q}_2})\right).\end{aligned} \tag{16}$$

The transition amplitudes in the prior form and in the post form are equal to one another when the potential and the wave function of quark-antiquark relative motion are those used in the Schrödinger equation [63–65]. Otherwise, $\mathcal{M}_{\rm fi}^{\rm prior}\neq\mathcal{M}_{\rm fi}^{\rm post}$ for inelastic scattering. The inequality yields different cross sections corresponding to the two forms, which is the so-called post-prior discrepancy [63–65].

In the Schrödinger equation we have only used the central spin-independent potential in Eq. (5) since the spin-spin interaction in Eq. (10) contains the delta function that can not be correctly dealt with in the equation. But in the transition amplitudes where the Fourier transform of the spin-spin interaction can be correctly dealt with, we use

the Fourier transform of both the central spin-independent potential and the spin-spin interaction:

$$\begin{aligned} V_{ab}\left(\vec{Q}\right) &= -\frac{\vec{\lambda}_a}{2}\cdot\frac{\vec{\lambda}_b}{2}\frac{3}{4}D\left[1.3-\left(\frac{T}{T_c}\right)^4\right]\left[(2\pi)^3\delta^3(\vec{Q})-\frac{8\pi}{Q}\int_0^\infty dr\frac{r\sin(Qr)}{\exp(2Ar)+1}\right] \\ &+\frac{\vec{\lambda}_a}{2}\cdot\frac{\vec{\lambda}_b}{2}64\pi E\int_0^\infty dq\frac{\rho(q^2)-\frac{K}{q^2}}{(E^2+Q^2+q^2)^2-4Q^2q^2} \\ &-\frac{\vec{\lambda}_a}{2}\cdot\frac{\vec{\lambda}_b}{2}\frac{16\pi^2}{25}\frac{\vec{s}_a\cdot\vec{s}_b}{m_a m_b}+\frac{\vec{\lambda}_a}{2}\cdot\frac{\vec{\lambda}_b}{2}\frac{16\pi^2\lambda}{25Q}\int_0^\infty dx\frac{d^2v\,(x)}{dx^2}\sin\left(\frac{Q}{\lambda}x\right)\frac{\vec{s}_a\cdot\vec{s}_b}{m_a m_b}. \end{aligned} \tag{17}$$

Therefore, the post-prior discrepancy occurs in our calculations. We take the average of the cross section in the prior form and the one in the post form. Each of the two cross sections related to the prior form and the post form is the unpolarized cross section obtained from the cross section in Eq. (14)

$$\sigma^{\rm unpol}(\sqrt{s})=\frac{1}{(2S_A+1)(2S_B+1)}\sum_S(2S+1)\sigma(S,m_S,\sqrt{s}), \tag{18}$$

where S_A and S_B are the spins of A and B, respectively, and S is the total spin of the two mesons allowed by the reaction $A+B\to C+D$. The cross section $\sigma^{\rm unpol}(\sqrt{s})$ is independent of the magnetic projection quantum number m_S of S.

4. Numerical results and discussions

The quark masses $m_{\rm u}=m_{\rm d}=0.32$ GeV and $m_{\rm s}=0.5$ GeV determined in the fit to the experimental mass splittings in Section 2 are kept unchanged in hadronic matter. They are used in the Schrödinger equation with the central spin-independent but temperature-dependent potential in Eq. (5). The lowest-energy S-wave solution of the Schrödinger equation is a temperature-dependent radial wave function of the quark-antiquark relative motion of mesons in the ground-state pseudoscalar octet and the ground-state vector nonet. When the temperature increases, the peak of r times the S-wave radial wave function, $rR_{q\bar{q}}(T,r)$, moves to larger quark-antiquark distances and the meson's root-mean-square radius increases. This reflects the phenomenon that with increasing temperature any bound state becomes looser and looser while confinement gets weaker, i.e. the poten-

tial plateau at large distances decreases with increasing temperature and a higher plateau begins at a larger distance.

Another consequence of the temperature-dependent potential in Eq. (5) is that masses of π, ρ, K and K^* decrease with increasing temperature in the region $0.6 \leq T/T_c \leq 0.99$. The mass splitting of a spin-0 meson and a spin-1 meson with the same isospin is calculated according to

$$< V_{\rm ss} >= \frac{16\pi}{75 m_a m_b}[R^2_{q\bar{q}}(T, r=0) - \int_0^\infty dr r \frac{d^2 v(\lambda r)}{dr^2} R^2_{q\bar{q}}(T, r)]. \tag{19}$$

The spin-averaged mass of a spin-0 meson and a spin-1 meson with the same isospin is one-fourth of the spin-0 meson mass plus three-fourths of the spin-1 meson mass [3]. The spin-averaged mass of π and ρ equals the sum of quark mass, antiquark mass and the energy of the relative motion obtained from the Schrödinger equation. Since for the quark-antiquark relative motion we take the same spatial wave functions of K and K^* as that of π and ρ mesons, the spin-averaged mass of K and K^* equals the sum of quark mass, antiquark mass and the nonrelativistic-Hamiltonian expectation value of the wave function. After mass splittings and spin-averaged masses are obtained, we find meson masses of which the mass of the spin-0 meson is the spin-averaged mass minus three-fourths of the mass splitting of the spin-0 and spin-1 mesons, and the mass of the spin-1 meson is the spin-averaged mass plus one-fourth of the mass splitting. The temperature-dependent meson masses are plotted in Fig. 2. The reason for the falloff of masses with increasing temperature is that the first term of the potential related to the large-distance plateau gives a smaller contribution at higher temperature. When $T \to T_c$, the masses of the π and ρ mesons approach 0 and 0.006 GeV, respectively. This indicates that the π and ρ mesons are almost massless at a temperature very close to T_c. In addition to the falloff of masses, the mass splitting of π and ρ and the one of K and K^* are both close to zero at $T \to T_c$. When $T \to T_c$, the masses of K and K^* approach finite values 0.179 GeV and 0.183 GeV, respectively. The kaons and vector kaons become degenerate in mass near T_c. Similar to Ref. [3], a constant of 0.88857 GeV is subtracted from the energy of the Schrödinger equation for π and ρ and from the nonrelativistic-Hamiltonian expectation

value of the wave function for K and K^*. This subtraction makes the theoretical values of the spin-averaged masses at $T = 0$ approach the experimental data and the masses of π and ρ go to zero at $T \to T_c$. The subtraction does not influence the sizes of meson bound states and the mass splittings.

The meson masses in units of GeV are parametrized as

$$m_\pi = 0.41 \left[1 - \left(\frac{T}{1.05T_c}\right)^{11.88}\right]^{3.81}, \tag{20}$$

$$m_\rho = 0.7 \left[1 - \left(\frac{T}{T_c}\right)^{4.29}\right]^{1.14}, \tag{21}$$

$$m_K = 0.63 \left[1 - \left(\frac{T}{1.15T_c}\right)^{9.31}\right]^{4.4}, \tag{22}$$

$$m_{K^*} = 0.84 \left[1 - \left(\frac{T}{1.05T_c}\right)^{4.16}\right], \tag{23}$$

which are valid in the region $0.6 \leq T/T_c \leq 0.99$. Since the temperature of hadronic matter is generally larger than 0.11 GeV and smaller than T_c, the meson masses and cross sections shown in the next paragraph in the temperature region are sufficient for studies concerned with hadronic matter.

The wave function of quark-antiquark relative motion of the π and ρ mesons is taken to be the same as those of the other ground-state mesons. With $m_{\rm u} = m_{\rm d} = 0.32$ GeV obtained in Section 2, the experimental data of S-wave $I = 2$ elastic phase shifts for $\pi\pi$ scattering in vacuum [66–69] are reproduced with the potential in Eq. (17). Keeping quark masses at the values determined in the fit to the experimental mass splittings, the dependence of the transition amplitude $\mathcal{M}_{\rm fi}$ on temperature comes from the wave function, the potential in Eq. (17) and the meson masses. The transition amplitude contains also color, spin and flavor matrices that are not affected by the temperature. Since the meson masses depend on temperature, threshold energies for inelastic meson-meson scattering depend on temperature. The temperature dependence of the potential, the quark-antiquark wave function and the meson masses leads to temperature-dependent cross sections for inelastic meson-meson scattering. Unpolarized cross sections for the

seven reactions $\pi\pi \to \rho\rho$ for $I = 2$, $KK \to K^*K^*$ for $I = 1$, $KK^* \to K^*K^*$ for $I = 1$, $\pi K \to \rho K^*$ for $I = 3/2$, $\pi K^* \to \rho K^*$ for $I = 3/2$, $\rho K \to \rho K^*$ for $I = 3/2$, and $\pi K^* \to \rho K$ for $I = 3/2$ are plotted in Figs. 3-9. For convenient application the numerical cross sections are parametrized as

$$\begin{aligned} \sigma^{\rm unpol} &= a_1 \left(\frac{\sqrt{s} - \sqrt{s_0}}{b_1} \right)^{c_1} \exp\left[c_1 \left(1 - \frac{\sqrt{s} - \sqrt{s_0}}{b_1} \right) \right] \\ &\quad + a_2 \left(\frac{\sqrt{s} - \sqrt{s_0}}{b_2} \right)^{c_2} \exp\left[c_2 \left(1 - \frac{\sqrt{s} - \sqrt{s_0}}{b_2} \right) \right]. \end{aligned} \tag{24}$$

Time-consuming computations determine values of the parameters a_1, b_1, c_1, a_2, b_2 and c_2, which are shown in Tables 2 and 3.

At the threshold energy of an endothermic reaction at a given temperature the momenta of final mesons in the center-of-mass frame equal zero. It is shown by Eqs. (12) and (13) that the absolute values of the momenta of initial and final mesons ($\mid \vec{P} \mid$ and $\mid \vec{P}' \mid$) increase as $\sqrt{s}$ increases. The rise of $\mid \vec{P}' \mid$ causes a rapid increase of the cross section close to the threshold energy. The relative momentum $\vec{p}_{ab}$ is a linear combination of $\vec{P}$ and $\vec{P}'$. Thus, $\mid \vec{p}_{ab} \mid$ increases with increasing $\sqrt{s}$, while $\psi_{ab}(\vec{p}_{ab})$ is reduced by the increase of $\mid \vec{p}_{ab} \mid$. The wave function $\psi_{ab}(\vec{p}_{ab})$ and the absolute value of the transition amplitude $\mid \mathcal{M}_{\rm fi} \mid$ thus decrease with increasing $\sqrt{s}$. This decreases the cross section with increasing $\sqrt{s}$. The rising $\mid \vec{P}' \mid$ and falling $\psi_{ab}(\vec{p}_{ab})$ produce a peak in the cross section near the threshold energy. At a higher temperature the constituents a and b have larger support of relative motion in coordinate space and so $\psi_{ab}(\vec{p}_{ab})$ gets narrower in momentum space. This results in a cross section that decreases faster from the peak and forms a more narrow peak. The exception is that the width of the peak of a reaction at $T/T_c = 0.95$ is equal to or slightly larger than the one of the same reaction at $T/T_c = 0.9$.

Cross sections for the seven reactions in Figs. 3-9 indicate that peak cross sections increase from $T/T_c = 0$ to 0.65 but decrease from $T/T_c = 0.9$ to 0.95. While the temperature increases from zero, the potential plateau at large distances appears and moves lower. The Schrödinger equation with the potential produces increasing meson radii. Peak cross sections increase from $T/T_c = 0$ to 0.65 as the radii of initial mesons increase. While temperature goes to a higher value, bound states of mesons become looser due to

weaker confinement. At a temperature near T_c the bound states are very loose. Even though mesons are easily broken in the reaction $A(q_1\overline{q}_1) + B(q_2\overline{q}_2) \to C(q_1\overline{q}_2) + D(q_2\overline{q}_1)$ as $T/T_c \to 1$, it is more difficult to combine final quarks and antiquarks into mesons through quark rearrangement. Hence, peak cross sections decrease from $T/T_c = 0.9$ to 0.95. On the one hand larger radii of initial mesons cause larger cross sections for the meson-meson nonresonant reactions, on the other hand looser bound states of final mesons lead to smaller cross sections. When temperature increases, both factors generate rising or falling peak cross sections.

We may divide the seven reactions into three classes. The first class consists of the three reactions $\pi\pi \to \rho\rho$ for $I = 2$, $KK \to K^*K^*$ for $I = 1$ and $\pi K \to \rho K^*$ for $I = 3/2$ which have spin 0 for the two initial mesons and spin 1 for the two final mesons. The two maxima of the peak cross sections for the reactions are located at $T/T_c = 0.9$ and 0.75, respectively. The second class is just the reaction $\pi K^* \to \rho K$ for $I = 3/2$ which has spin 0 for an initial meson and a final meson and spin 1 for the others. The maximum of the peak cross section is located at $T/T_c = 0.85$. The third class is comprised of the three reactions $KK^* \to K^*K^*$ for $I = 1$, $\pi K^* \to \rho K^*$ for $I = 3/2$ and $\rho K \to \rho K^*$ for $I = 3/2$ which have spin 0 for an initial meson and spin 1 for the others. The maximum of the peak cross sections for these reactions is located at $T/T_c = 0.65$ or 0.75. In the first or third class the meson-flavor dependence of masses distinguishes the peak values of the three reactions at a given temperature. In the first class the difference of the total mass of the initial mesons and the total mass of the final mesons is larger than the ones in the other classes. When T/T_c changes from 0.6 to 0.99, the mass difference of the first class is reduced faster than the other two classes. The quicker reduction causes a more rapid increase of the peak value so that another maximum of the peak cross sections appears at $T/T_c = 0.9$ in addition to the maximum at $T/T_c = 0.75$.

The potential in Eq. (5) results from the interpolation between the potential of perturbative QCD at $r < 0.01$ fm and the lattice gauge results at large distances. The interpolation is in fact this procedure of adjusting the parameters A and E. We now begin to examine the sensitivity of mass splittings at $T = 0$ GeV, temperature-dependent

meson masses and cross sections to the interpolation procedure by adopting two new sets of A and E. The first set (named Set I) is obtained by reducing A in Eq. (6) by 5% and increasing E in Eq. (7) by 10% while the second set (named Set II) is obtained by increasing A in Eq. (6) by 5% and reducing E in Eq. (7) by 10%. The two new sets give good fits to the lattice gauge results. Mass splittings at $T = 0$ GeV and meson masses at five temperatures resulted from the two sets are listed in Tables 4 and 5, respectively. The change of the mass splittings or of the meson masses from Eqs. (6) and (7) to Set I or Set II is very small. The largest change in meson mass is 2.88% at $T = 0.65T_c$. But such a change only leads to negligible changes in cross section. For example, the peak cross section obtained from Set I for $KK \to K^*K^*$ for $I = 1$ at $T/T_c = 0.65$ is 1.2735 mb in comparison to the value 1.2686 mb obtained from Eqs. (6) and (7), and the peak cross section obtained from Set II for $\pi K \to \rho K^*$ for $I = 3/2$ at $T/T_c = 0.65$ is 0.4787 mb very close to the value 0.4930 mb resulted from Eqs. (6) and (7). Eventually, we understand that the mass splittings at $T = 0$ GeV, the temperature-dependent masses and the cross sections are not sensitive to the interpolation procedure for the construction of the potential given in Eq. (5).

In Figs. 3-9 we plot the average of the cross section in the prior form and the one in the post form. To see the uncertainty in this prescription, as an example, we draw in Fig. 10 cross sections obtained in the prior form and in the post form for the reaction $\pi\pi \to \rho\rho$ for $I = 2$. The solid curves in Fig. 3 are between the dashed curves corresponding to the prior form and the dotted curves corresponding to the post form. At a given temperature the dashed curve and the dotted curve almost overlap at the center-of-mass energies very close to or far away from the threshold energy. The post-prior discrepancy can be clearly marked by the difference of peak cross sections obtained in the two forms. We thus list the peak cross sections in Tables 6-8. The three tables are enough to display the discrepancy. Denote the peak cross section obtained in the prior (post) form by $\sigma_{\rm max}^{\rm prior}$ ($\sigma_{\rm max}^{\rm post}$). To indicate the discrepancy, we define

$$\chi = \frac{\sigma_{\rm max}^{\rm prior} - \sigma_{\rm max}^{\rm post}}{\sigma_{\rm max}^{\rm prior} + \sigma_{\rm max}^{\rm post}} \tag{25}$$

Since $\sigma_{\rm max}^{\rm prior} > 0$ and $\sigma_{\rm max}^{\rm post} > 0$, the values of χ are between -1 and 1. The smaller the absolute value of χ, the smaller the discrepancy. If χ is positive, $\sigma_{\rm max}^{\rm prior} > \sigma_{\rm max}^{\rm post}$; otherwise, $\sigma_{\rm max}^{\rm prior} \leq \sigma_{\rm max}^{\rm post}$. The quantity χ is also presented in Tables 6-8. From Fig. 10 we note that the peak cross sections obtained in the two forms at a given temperature may not correspond to the same center-of-mass energy.

5. Summary

We have given the temperature-dependent central-spin-independent potential that interpolates between the perturbative-QCD potential with loop corrections at short distances and the potential data offered by lattice gauge calculations at large distances. From the potential we obtain: (1) experimental mass splittings of the ground-state mesons with the same isospin when the masses of up, down and strange quarks are determined; (2) meson masses that decrease from $T/T_c = 0.6$ to 0.99; (3) the wave function of quark-antiquark relative motion that occupies a larger volume at a higher temperature. In the quark-interchange mechanism we have obtained cross sections for seven nonresonant reactions $\pi\pi \to \rho\rho$ for $I = 2$, $KK \to K^*K^*$ for $I = 1$, $KK^* \to K^*K^*$ for $I = 1$, $\pi K \to \rho K^*$ for $I = 3/2$, $\pi K^* \to \rho K^*$ for $I = 3/2$, $\rho K \to \rho K^*$ for $I = 3/2$ and $\pi K^* \to \rho K$ for $I = 3/2$. The temperature dependence of the cross sections is determined by the temperature dependence of the potential, the quark-antiquark wave function and the meson masses. Peak cross sections are affected by three factors: larger sizes of initial mesons at a higher temperature give larger peak cross sections, looser bound states of final mesons at a higher temperature lead to smaller peak cross sections, and a smaller total-mass difference of the initial mesons and the final mesons yields larger peak cross sections. The numerical cross sections are parametrized for future studies.

Acknowledgements

This work was supported in part by the National Natural Science Foundation of China under Grant No. 10675079 and in part by Shanghai Leading Academic Discipline Project

(project number S30105). We thank H. J. Weber for a careful reading of the manuscript.

References

[1] T. Barnes, E.S. Swanson, Phys. Rev. D 46 (1992) 131.

[2] E.S. Swanson, Ann. Phys. (N.Y.) 220 (1992) 73.

[3] K. Martins, D. Blaschke, E. Quack, Phys. Rev. C 51 (1995) 2723.

[4] C.-Y. Wong, E.S. Swanson, T. Barnes, Phys. Rev. C 65 (2001) 014903.

[5] T. Barnes, E.S. Swanson, C.-Y. Wong, X.-M. Xu, Phys. Rev. C 68 (2003) 014903.

[6] X.-M. Xu, Nucl. Phys. A 697 (2002) 825.

[7] D. Kharzeev, H. Satz, Phys. Lett. B 334 (1994) 155.

[8] M.E. Peskin, Nucl. Phys. B 156 (1979) 365.

[9] G. Bhanot, M.E. Peskin, Nucl. Phys. B 156 (1979) 391.

[10] F.D. Duraes, et al., Phys. Rev. C 68 (2003) 035208.

[11] S.G. Matinyan, B. Müller, Phys. Rev. C 58 (1998) 2994.

[12] Z. Lin, C.M. Ko, J. Phys. G 27 (2001) 617.

[13] K. Haglin, Phys. Rev. C 61 (2000) 031902.

[14] K. Haglin, C. Gale, Phys. Rev. C 63 (2001) 065201.

[15] Y. Oh, T. Song, S.H. Lee, Phys. Rev. C 63 (2001) 034901.

[16] S.S. Adler, et al., PHENIX Collaboration, Phys. Rev. C 69 (2004) 034909.

[17] I. Arsene, et al., BRAHMS Collaboration, Nucl. Phys. A 757 (2005) 1.

[18] B.B. Back, et al., PHOBOS Collaboration, Nucl. Phys. A 757 (2005) 28.

[19] J. Adams, et al., STAR Collaboration, Nucl. Phys. A 757 (2005) 102.

[20] K. Adcox, et al., PHENIX Collaboration, Nucl. Phys. A 757 (2005) 184.

[21] J. Adams, et al., STAR Collaboration, Phys. Rev. Lett. 92 (2004) 092301.

[22] I.G. Bearden, et al., BRAHMS Collaboration, Phys. Rev. Lett. 90 (2003) 102301.

[23] I.G. Bearden, et al., BRAHMS Collaboration, Phys. Rev. Lett. 94 (2005) 162301.

[24] Y.-Q. Li, X.-M. Xu, Nucl. Phys. A 794 (2007) 210.

[25] F. Karsch, E. Laermann, A. Peikert, Nucl. Phys. B 605 (2001) 579.

[26] I. Bender, H.G. Dosch, H.J. Pirner, H.G. Kruse, Nucl. Phys. A 414 (1984) 359.

[27] M. Döring, K. Hübner, O. Kaczmarek, F. Karsch, Phys. Rev. D 75 (2007) 054504.

[28] S. Gupta, K. Hübner, O. Kaczmarek, Phys. Rev. D 77 (2008) 034503.

[29] C. Michael, arXiv:hep-ph/9809211.

[30] G.S. Bali, A. Pineda, Phys. Rev. D 69 (2004) 094001.

[31] T. Sjöstrand, Comput. Phys. Commun. 39 (1986) 347.

[32] H. Miyazawa, Phys. Rev. D 20 (1979) 2953.

[33] V. Goloviznin, H. Satz, Yad. Fiz. 60N3 (1997) 523.

[34] H. Satz, hep-ph/0602245.

[35] O. Kaczmarek, F. Karsch, P. Petreczky, F. Zantow, Phys. Lett. B 543 (2002) 41.

[36] F. Zantow, O. Kaczmarek, F. Karsch, P. Petreczky, hep-lat/0301015.

[37] H. Satz, arXiv:0812.3829.

[38] L. Kluberg, H. Satz, arXiv:0901.3831.

[39] S. Digal, P. Petreczky, H. Satz, Phys. Lett. B 514 (2001) 57.

[40] E. Shuryak, I. Zahed, Phys. Rev. D 70 (2004) 054507.

[41] C.-Y. Wong, Phys. Rev. C 72 (2005) 034906.

[42] C.-Y. Wong, hep-ph/0509088.

[43] C.-Y. Wong, Phys. Rev. C 76 (2007) 014902.

[44] W.M. Alberico, A. Beraudo, A. De Pace, A. Molinari, Phys. Rev. D 72 (2005) 114011.

[45] H. Satz, J. Phys. G 32 (2006) R25.

[46] W. Buchmüller, S.-H.H. Tye, Phys. Rev. D 24 (1981) 132.

[47] C.-Y. Wong, Phys. Rev. C 65 (2002) 034902.

[48] A. De Rújula, H. Georgi, S.L. Glashow, Phys. Rev. D 12 (1975) 147.

[49] N. Isgur, G. Karl, Phys. Rev. D 18 (1978) 4187.

[50] N. Isgur, G. Karl, Phys. Rev. D 19 (1979) 2653.

[51] N. Isgur, G. Karl, Phys. Rev. D 20 (1979) 1191.

[52] S. Godfrey, N. Isgur, Phys. Rev. D 32 (1985) 189.

[53] S. Capstick, N. Isgur, Phys. Rev. D 34 (1986) 2809.

[54] Z.V. Chraplyvy, Phys. Rev. 91 (1953) 388.

[55] J.D. Bjorken, S.D. Drell, Relativistic Quantum Mechanics, McGraw-Hill, New York, 1964.

[56] S. Weinberg, The Quantum Theory of Fields, Vol. II, Cambridge University Press, Cambridge, 1996.

[57] S. Pokorski, Gauge Field Theories, Cambridge University Press, Cambridge, 2000.

[58] J.F. Donoghue, E. Golowich, B.R. Holstein, Dynamics of the Standard Model, Cambridge University Press, Cambridge, 1992.

[59] J. Gasser, H. Leutwyler, Ann. Phys. 158 (1984) 142.

[60] J. Gasser, H. Leutwyler, Nucl. Phys. B 250 (1985) 465.

[61] J. Bijnens, G. Colangelo, G. Ecker, J. Gasser, M.E. Sainio, Nucl. Phys. B 508 (1997) 263.

[62] G. Colangelo, J. Gasser, H. Leutwyler, Nucl. Phys. B 603 (2001) 125.

[63] N.F. Mott, H.S.W. Massey, The Theory of Atomic Collisions, Clarendon Press, Oxford, 1965.

[64] T. Barnes, N. Black, E.S. Swanson, Phys. Rev. C 63 (2001) 025204.

[65] C.-Y. Wong, H.W. Crater, Phys. Rev. C 63 (2001) 044907.

[66] E. Colton, et al., Phys. Rev. D 3 (1971) 2028.

[67] N.B. Durusoy, et al., Phys. Lett. B 45 (1973) 517.

[68] W. Hoogland, et al., Nucl. Phys. B 126 (1977) 109.

[69] M.J. Losty, et al., Nucl. Phys. B 69 (1974) 185.

Table 1: Vacuum masses of π, ρ, K and K^* and their spin-averaged masses.

	$\overline{m}_{\pi\rho}$ (GeV)	m_π (GeV)	m_ρ (GeV)	$\overline{m}_{KK^*}$ (GeV)	m_K (GeV)	m_{K^*} (GeV)
model	0.7112	0.2620	0.8609	0.8339	0.5465	0.9298
experiment	0.6124	0.1396	0.7700	0.7929	0.4957	0.8920

Table 2: Values of parameters in the parametrization given in Eq. (24).

reaction	T/T_c	a_1 (mb)	b_1 (GeV)	c_1	a_2 (mb)	b_2 (GeV)	c_2
$I=2$ $\pi\pi \to \rho\rho$	0.65	0.52	0.13	2.47	0.07	0.04	0.42
$I=2$ $\pi\pi \to \rho\rho$	0.75	0.86	0.13	3.11	0.35	0.04	0.71
$I=2$ $\pi\pi \to \rho\rho$	0.85	0.65	0.0075	0.38	0.97	0.12	1.93
$I=2$ $\pi\pi \to \rho\rho$	0.9	1.96	0.009	0.5	0.43	0.15	1.58
$I=2$ $\pi\pi \to \rho\rho$	0.95	1.03	0.017	0.47	0.18	0.28	3.55
$I=1$ $KK \to K^*K^*$	0.65	0.85	0.11	0.89	0.4	0.1	0.44
$I=1$ $KK \to K^*K^*$	0.75	1.42	0.09	1.14	0.46	0.15	0.39
$I=1$ $KK \to K^*K^*$	0.85	1	0.06	0.76	0.47	0.08	0.22
$I=1$ $KK \to K^*K^*$	0.9	1.3	0.005	0.63	0.72	0.04	0.23
$I=1$ $KK \to K^*K^*$	0.95	1.56	0.006	0.48	0.3	0.065	0.31
$I=1$ $KK^* \to K^*K^*$	0.65	1.71	0.09	0.58	0.66	0.1	2.64
$I=1$ $KK^* \to K^*K^*$	0.75	1.63	0.09	0.71	0.83	0.07	1.61
$I=1$ $KK^* \to K^*K^*$	0.85	0.88	0.038	0.57	0.49	0.1	0.49
$I=1$ $KK^* \to K^*K^*$	0.9	0.33	0.006	1.17	0.57	0.035	0.21
$I=1$ $KK^* \to K^*K^*$	0.95	0.51	0.006	0.47	0.24	0.05	0.28

Table 3: Values of parameters in the parametrization given in Eq. (24).

reaction	T/T_c	a_1 (mb)	b_1 (GeV)	c_1	a_2 (mb)	b_2 (GeV)	c_2
$I=\frac{3}{2}$ $\pi K \to \rho K^*$	0.65	0.3	0.01	0.89	0.48	0.16	1.45
$I=\frac{3}{2}$ $\pi K \to \rho K^*$	0.75	0.44	0.14	1.43	0.22	0.1	0.47
$I=\frac{3}{2}$ $\pi K \to \rho K^*$	0.85	0.09	0.006	0.001	0.41	0.093	0.96
$I=\frac{3}{2}$ $\pi K \to \rho K^*$	0.9	0.76	0.007	0.65	0.24	0.05	0.16
$I=\frac{3}{2}$ $\pi K \to \rho K^*$	0.95	0.55	0.012	0.59	0.09	0.03	0.15
$I=\frac{3}{2}$ $\pi K^* \to \rho K^*$	0.65	0.72	0.13	1.29	0.06	0.06	0.19
$I=\frac{3}{2}$ $\pi K^* \to \rho K^*$	0.75	0.74	0.11	0.93	0.05	0.04	0.42
$I=\frac{3}{2}$ $\pi K^* \to \rho K^*$	0.85	0.22	0.084	1.95	0.21	0.08	0.26
$I=\frac{3}{2}$ $\pi K^* \to \rho K^*$	0.9	0.25	0.007	0.63	0.19	0.05	0.24
$I=\frac{3}{2}$ $\pi K^* \to \rho K^*$	0.95	0.16	0.01	0.56	0.08	0.07	0.24
$I=\frac{3}{2}$ $\rho K \to \rho K^*$	0.65	0.7	0.001	2.65	1.1	0.12	1.2
$I=\frac{3}{2}$ $\rho K \to \rho K^*$	0.75	0.69	0.11	0.81	0.36	0.09	2.1
$I=\frac{3}{2}$ $\rho K \to \rho K^*$	0.85	0.1	0.11	0.12	0.36	0.07	0.84
$I=\frac{3}{2}$ $\rho K \to \rho K^*$	0.9	0.27	0.007	0.53	0.21	0.05	0.29
$I=\frac{3}{2}$ $\rho K \to \rho K^*$	0.95	0.09	0.045	0.14	0.09	0.03	4.54
$I=\frac{3}{2}$ $\pi K^* \to \rho K$	0.65	1.68	0.012	0.53	0.46	0.06	0.38
$I=\frac{3}{2}$ $\pi K^* \to \rho K$	0.75	2.12	0.01	0.76	0.66	0.01	0.09
$I=\frac{3}{2}$ $\pi K^* \to \rho K$	0.85	1.82	0.004	0.48	1.31	0.01	0.46
$I=\frac{3}{2}$ $\pi K^* \to \rho K$	0.9	1.6	0.005	0.42	0.29	0.03	0.68
$I=\frac{3}{2}$ $\pi K^* \to \rho K$	0.95	0.58	0.006	0.4	0.2	0.04	1.18

Table 4: Mass splittings in units of GeV at zero temperature.

	$m_\rho - m_\pi$	$m_{K^*} - m_K$	$\frac{1}{3}m_\omega + \frac{2}{3}m_\phi - m_\eta$
Eqs. (6) and (7)	0.5989	0.3833	0.3622
Set I	0.5890	0.3770	0.3530
Set II	0.6090	0.3898	0.3666

Table 5: Masses of π, ρ, K and K^* in units of GeV at various temperatures.

	T/T_c	m_π	m_ρ	m_K	m_{K^*}
Eqs. (6) and (7)	0.65	0.4042	0.5776	0.6161	0.7271
Eqs. (6) and (7)	0.75	0.3839	0.4710	0.5789	0.6347
Eqs. (6) and (7)	0.85	0.2958	0.3183	0.4776	0.4921
Eqs. (6) and (7)	0.9	0.2105	0.2221	0.3902	0.3976
Eqs. (6) and (7)	0.95	0.1021	0.1095	0.2809	0.2857
Set I	0.65	0.3926	0.5761	0.6063	0.7237
Set I	0.75	0.3775	0.4708	0.5736	0.6334
Set I	0.85	0.2956	0.3182	0.4774	0.4919
Set I	0.9	0.2110	0.2221	0.3905	0.3976
Set I	0.95	0.1026	0.1095	0.2813	0.2858
Set II	0.65	0.4118	0.5787	0.6162	0.7230
Set II	0.75	0.3873	0.4713	0.5791	0.6328
Set II	0.85	0.2952	0.3184	0.4772	0.4920
Set II	0.9	0.2098	0.2221	0.3899	0.3978
Set II	0.95	0.1014	0.1095	0.2807	0.2859

Table 6: Post-prior discrepancy

reaction	T/T_c	$\sigma_{\max}^{\text{prior}}$ (mb)	$\sigma_{\max}^{\text{post}}$ (mb)	χ
$I = 2\ \pi\pi \to \rho\rho$	0	0.5383	0.4443	0.0957
$I = 2\ \pi\pi \to \rho\rho$	0.65	0.6208	0.5157	0.0925
$I = 2\ \pi\pi \to \rho\rho$	0.75	1.2168	0.9064	0.1462
$I = 2\ \pi\pi \to \rho\rho$	0.85	1.2073	0.9010	0.1453
$I = 2\ \pi\pi \to \rho\rho$	0.9	1.6551	2.2077	-0.1431
$I = 2\ \pi\pi \to \rho\rho$	0.95	0.8296	1.2089	-0.1861
$I = 1\ KK \to K^*K^*$	0	0.5386	0.7257	-0.1480
$I = 1\ KK \to K^*K^*$	0.65	1.2308	1.3510	-0.0466
$I = 1\ KK \to K^*K^*$	0.75	1.8543	1.8601	-0.0016
$I = 1\ KK \to K^*K^*$	0.85	1.7125	1.3213	0.1289
$I = 1\ KK \to K^*K^*$	0.9	1.5737	2.2874	-0.1848
$I = 1\ KK \to K^*K^*$	0.95	1.5242	2.0874	-0.1559
$I = 1\ KK^* \to K^*K^*$	0	0.9475	0.9425	0.0026
$I = 1\ KK^* \to K^*K^*$	0.65	2.1129	2.6930	-0.1207
$I = 1\ KK^* \to K^*K^*$	0.75	2.3603	2.6151	-0.0512
$I = 1\ KK^* \to K^*K^*$	0.85	1.4742	1.1657	0.1169
$I = 1\ KK^* \to K^*K^*$	0.9	1.6670	0.0377	0.9558
$I = 1\ KK^* \to K^*K^*$	0.95	1.3724	0.0163	0.9765

Table 7: Post-prior discrepancy

reaction	T/T_c	$\sigma_{\max}^{\text{prior}}$ (mb)	$\sigma_{\max}^{\text{post}}$ (mb)	χ
$I = \frac{3}{2}\ \pi K \to \rho K^*$	0	0.3430	0.3615	-0.0263
$I = \frac{3}{2}\ \pi K \to \rho K^*$	0.65	0.5111	0.4830	0.0283
$I = \frac{3}{2}\ \pi K \to \rho K^*$	0.75	0.7084	0.6268	0.0611
$I = \frac{3}{2}\ \pi K \to \rho K^*$	0.85	0.6149	0.4901	0.1129
$I = \frac{3}{2}\ \pi K \to \rho K^*$	0.9	0.7691	1.1911	-0.2153
$I = \frac{3}{2}\ \pi K \to \rho K^*$	0.95	0.4953	0.7650	-0.2140
$I = \frac{3}{2}\ \pi K^* \to \rho K^*$	0	0.5415	0.4310	0.1136
$I = \frac{3}{2}\ \pi K^* \to \rho K^*$	0.65	0.7573	0.8279	-0.0445
$I = \frac{3}{2}\ \pi K^* \to \rho K^*$	0.75	0.8269	0.8191	0.0047
$I = \frac{3}{2}\ \pi K^* \to \rho K^*$	0.85	0.5147	0.4022	0.1227
$I = \frac{3}{2}\ \pi K^* \to \rho K^*$	0.9	0.6862	0.1273	0.6870
$I = \frac{3}{2}\ \pi K^* \to \rho K^*$	0.95	0.3985	0.0823	0.6576
$I = \frac{3}{2}\ \rho K \to \rho K^*$	0	0.6318	0.5553	0.0644
$I = \frac{3}{2}\ \rho K \to \rho K^*$	0.65	1.1125	1.1724	-0.0262
$I = \frac{3}{2}\ \rho K \to \rho K^*$	0.75	1.1026	1.0686	0.0157
$I = \frac{3}{2}\ \rho K \to \rho K^*$	0.85	0.5808	0.4368	0.1415
$I = \frac{3}{2}\ \rho K \to \rho K^*$	0.9	0.8565	0.0061	0.9859
$I = \frac{3}{2}\ \rho K \to \rho K^*$	0.95	0.4294	0.0080	0.9634

Table 8: Post-prior discrepancy

reaction	T/T_c	$\sigma_{\max}^{\text{prior}}$ (mb)	$\sigma_{\max}^{\text{post}}$ (mb)	χ
$I = \frac{3}{2}\ \pi K^* \to \rho K$	0	1.4320	1.1445	0.1116
$I = \frac{3}{2}\ \pi K^* \to \rho K$	0.65	2.7801	0.7960	0.5548
$I = \frac{3}{2}\ \pi K^* \to \rho K$	0.75	2.9691	1.1931	0.4267
$I = \frac{3}{2}\ \pi K^* \to \rho K$	0.85	3.3879	2.6925	0.1144
$I = \frac{3}{2}\ \pi K^* \to \rho K$	0.9	1.8472	1.7048	0.0401
$I = \frac{3}{2}\ \pi K^* \to \rho K$	0.95	0.6578	0.6441	0.0105

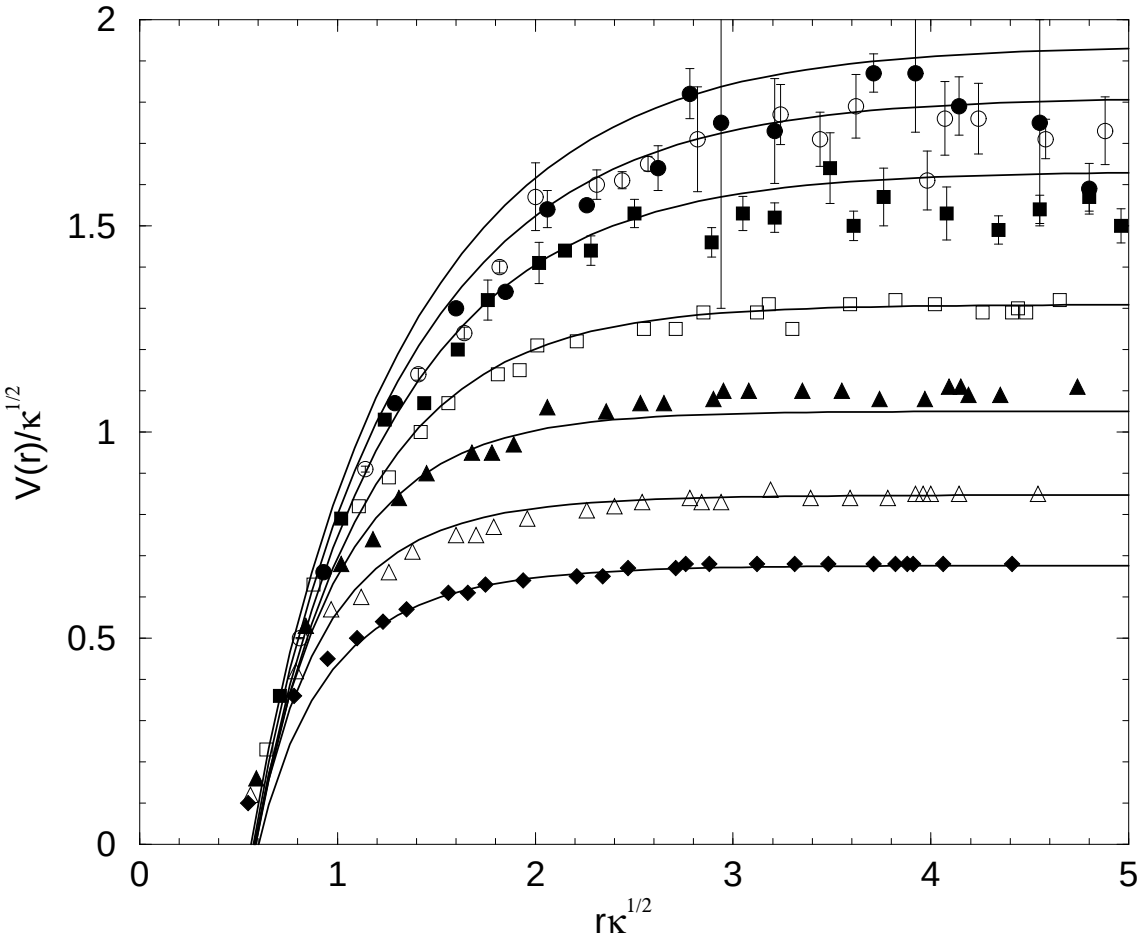

Figure 1: Temperature-dependent potential. From top to bottom the temperatures corresponding to the different data sets [25] are $T/T_c = 0.58,\ 0.66,\ 0.74,\ 0.84,\ 0.9,\ 0.94,\ 0.97$. Solid curves stand for the parametrization fitted to the data at these temperatures. $\sqrt{\kappa} = 2.154\ \mathrm{fm}^{-1} = 0.425\ \mathrm{GeV}$.

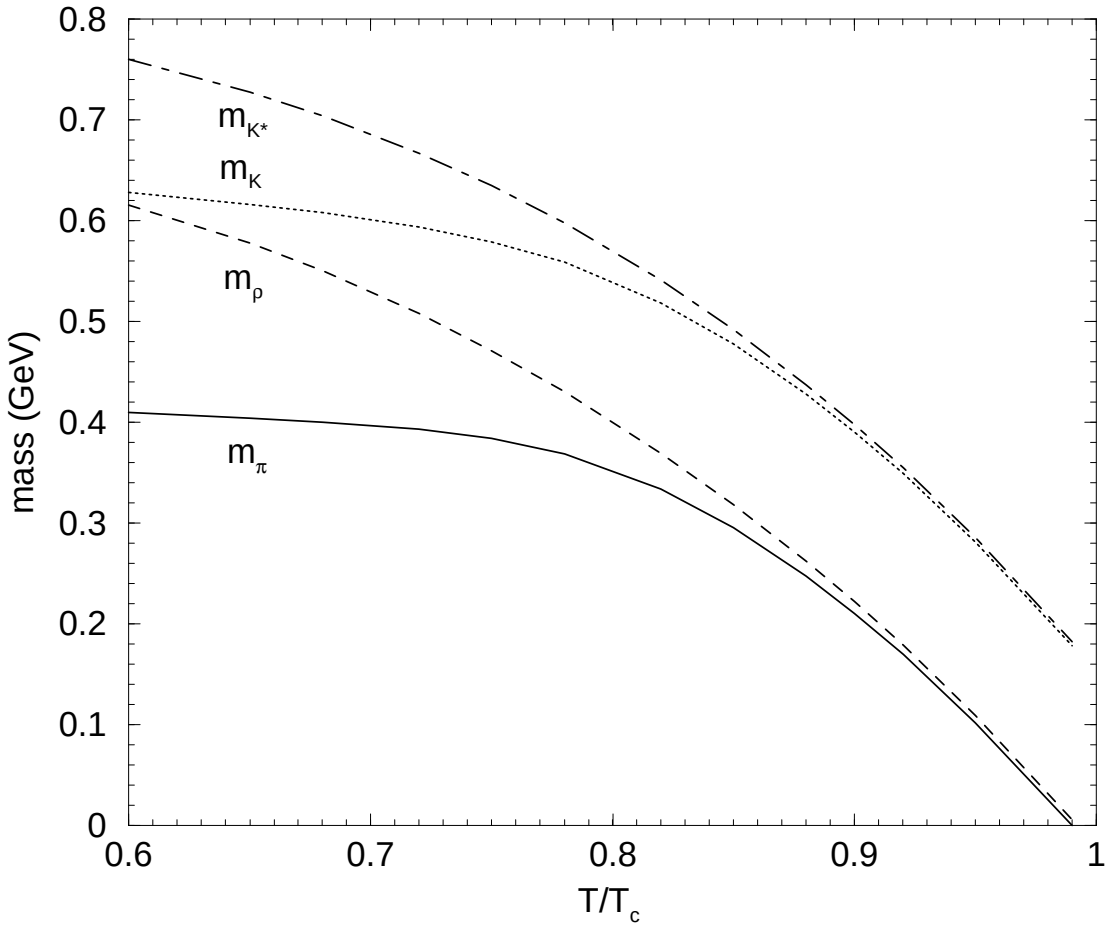

Figure 2: Meson masses as functions of T/T_c.

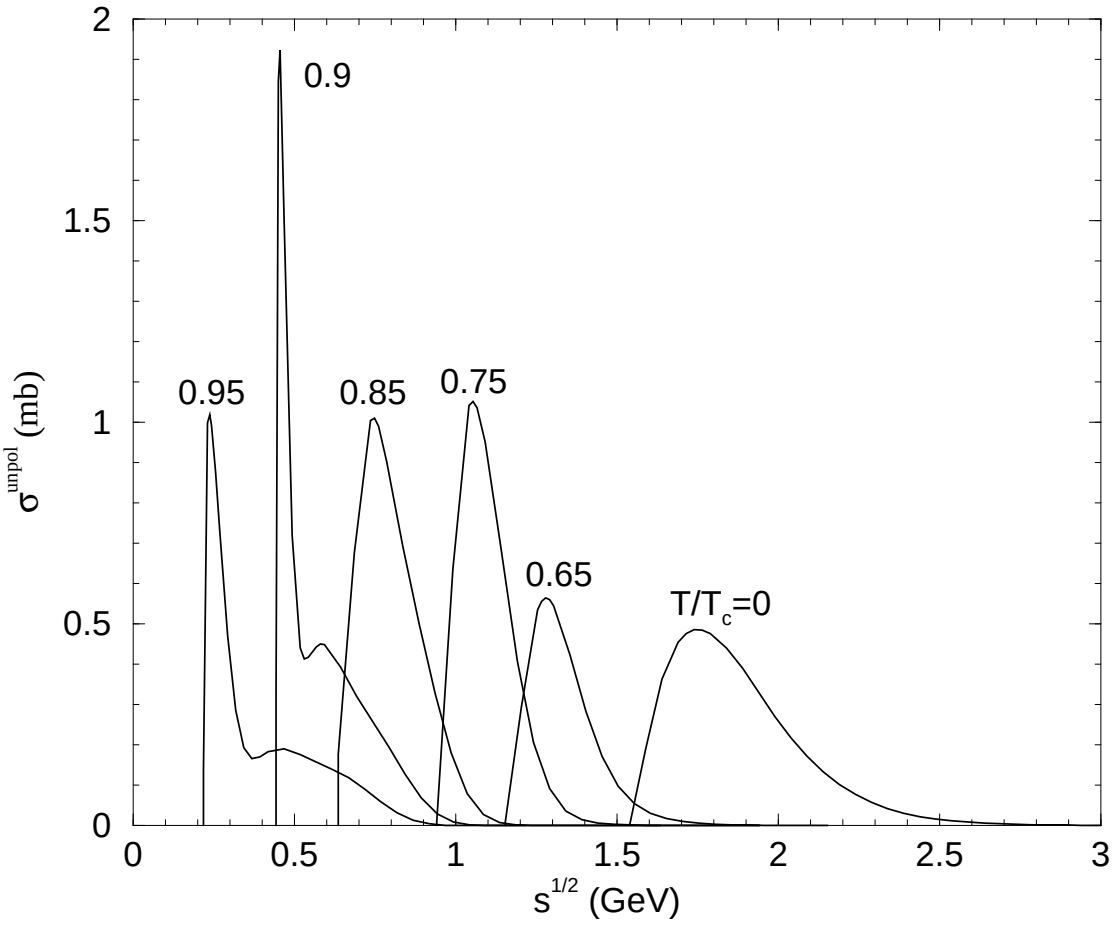

Figure 3: $\pi\pi \to \rho\rho$ cross sections for $I = 2$ at various temperatures.

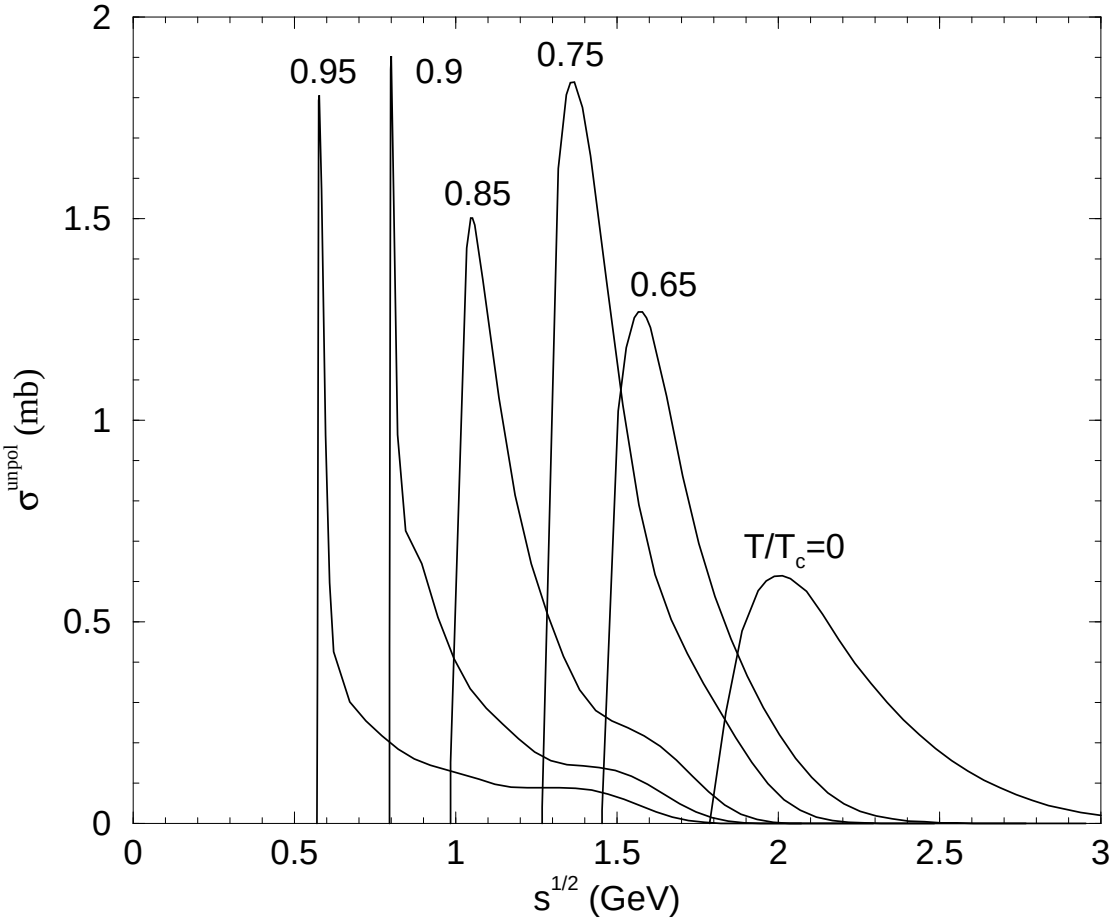

Figure 4: $KK \to K^*K^*$ cross sections for $I = 1$ at various temperatures.

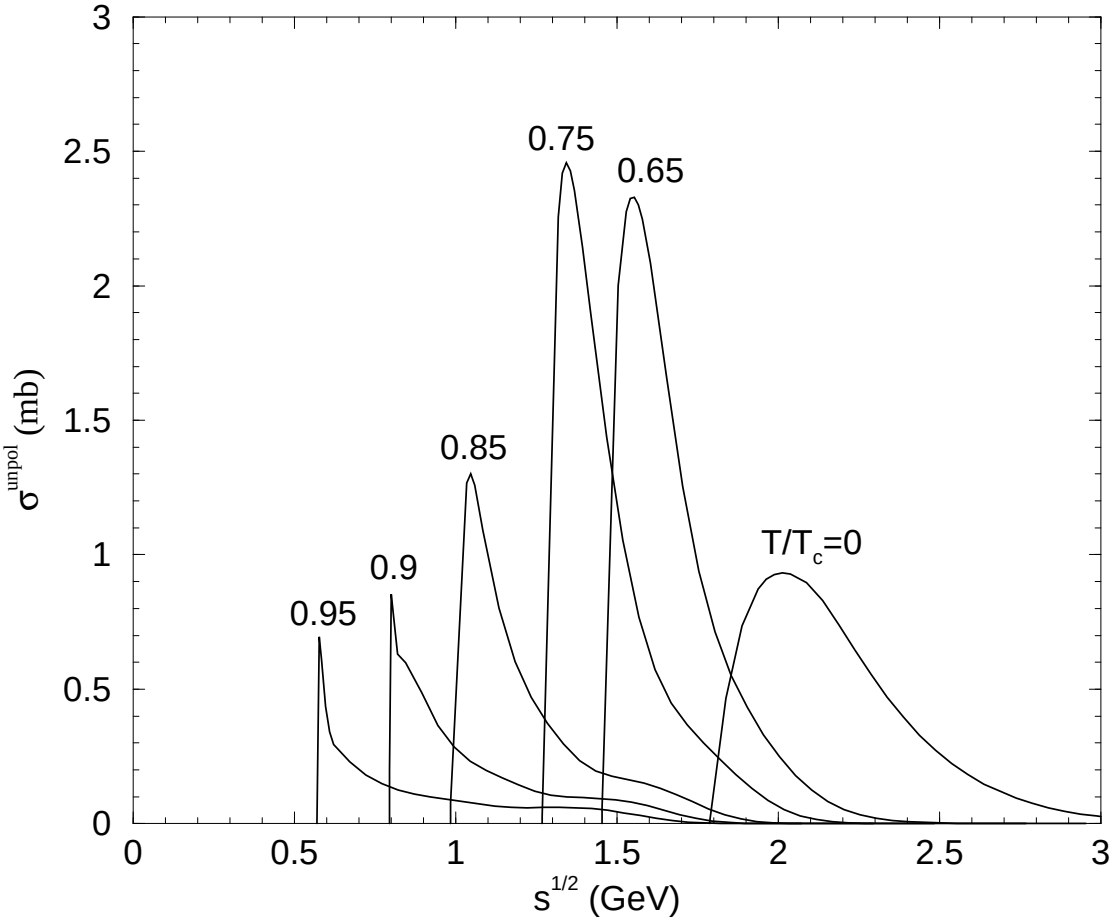

Figure 5: $KK^* \to K^*K^*$ cross sections for $I = 1$ at various temperatures.

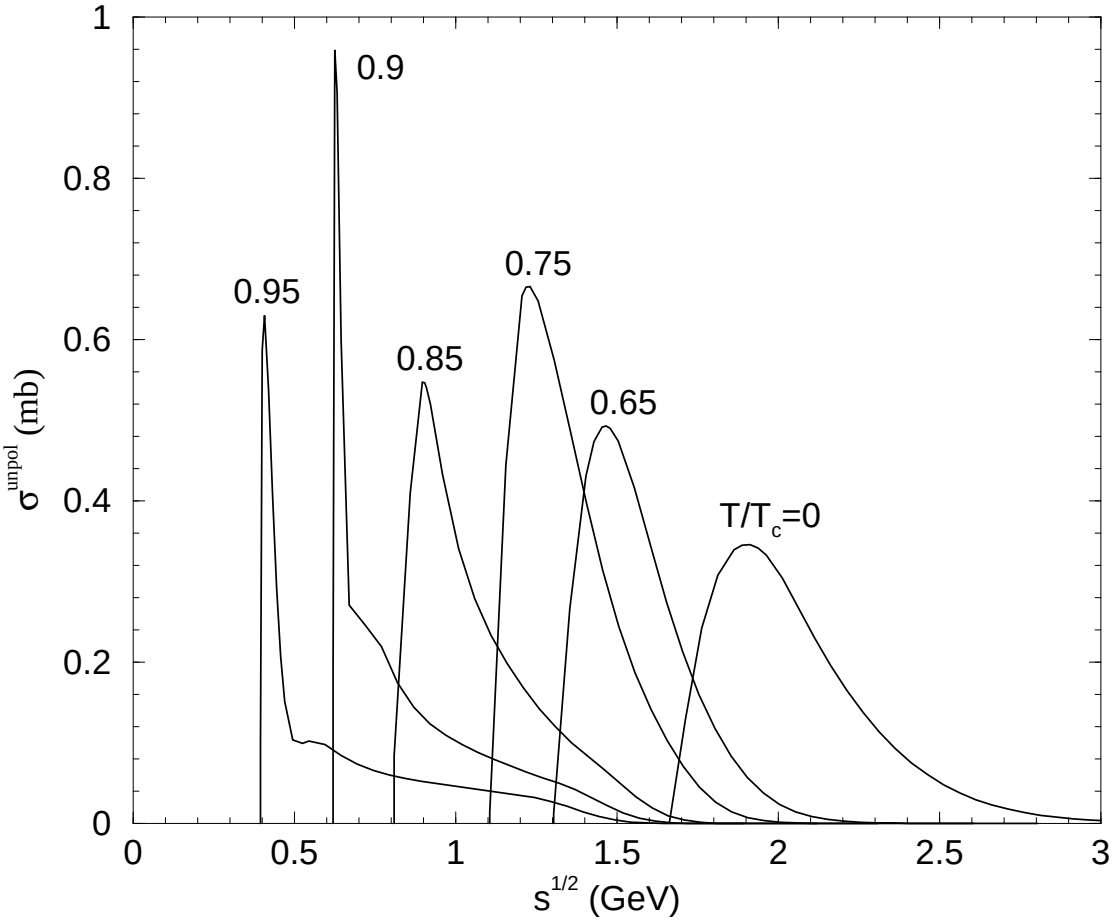

Figure 6: $\pi K \to \rho K^*$ cross sections for $I = 3/2$ at various temperatures.

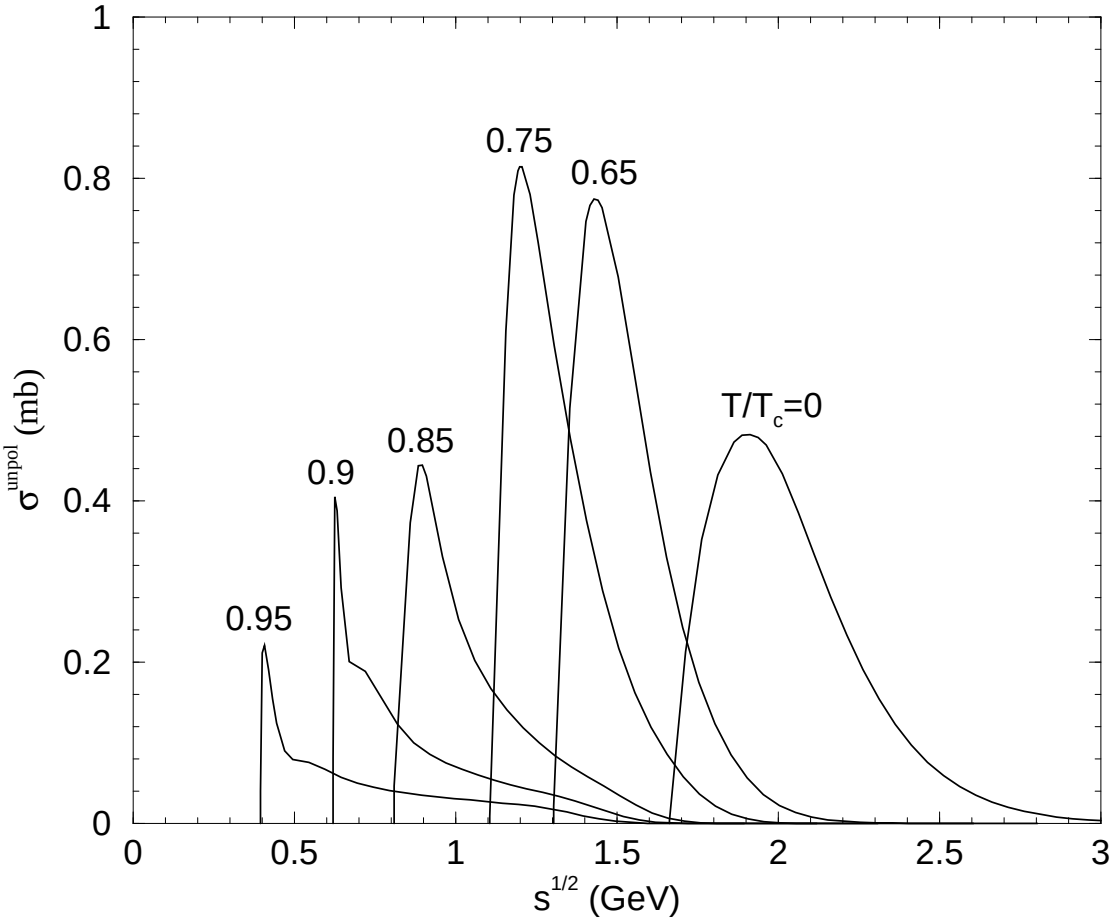

Figure 7: $\pi K^* \to \rho K^*$ cross sections for $I = 3/2$ at various temperatures.

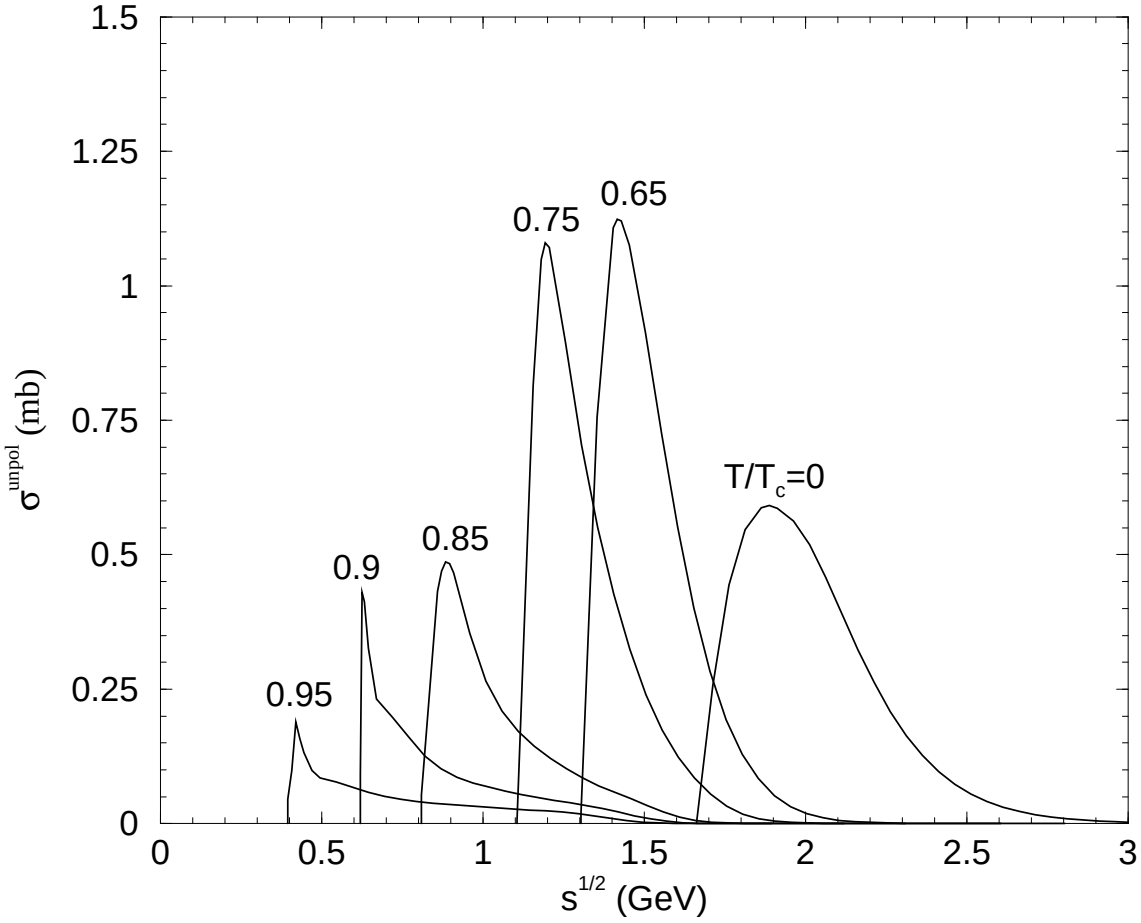

Figure 8: $\rho K \to \rho K^*$ cross sections for $I = 3/2$ at various temperatures.

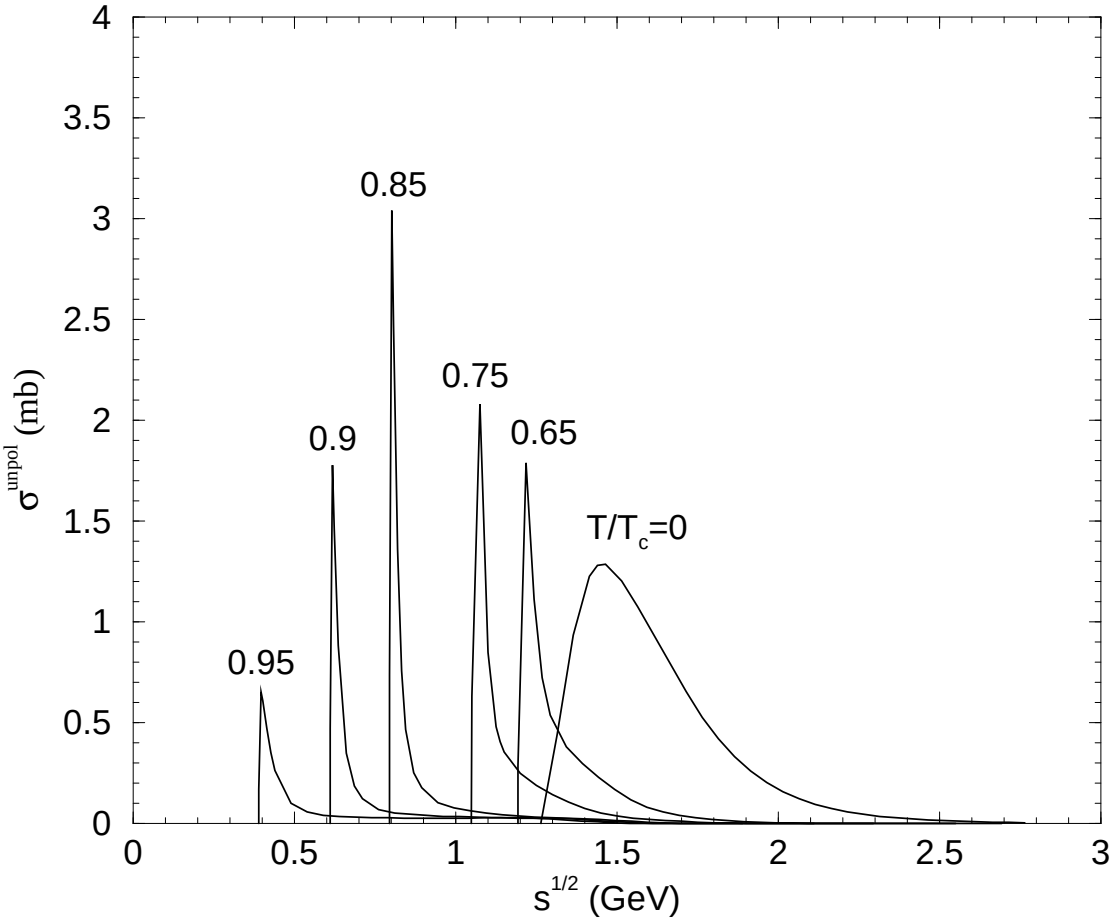

Figure 9: $\pi K^* \to \rho K$ cross sections for $I = 3/2$ at various temperatures.

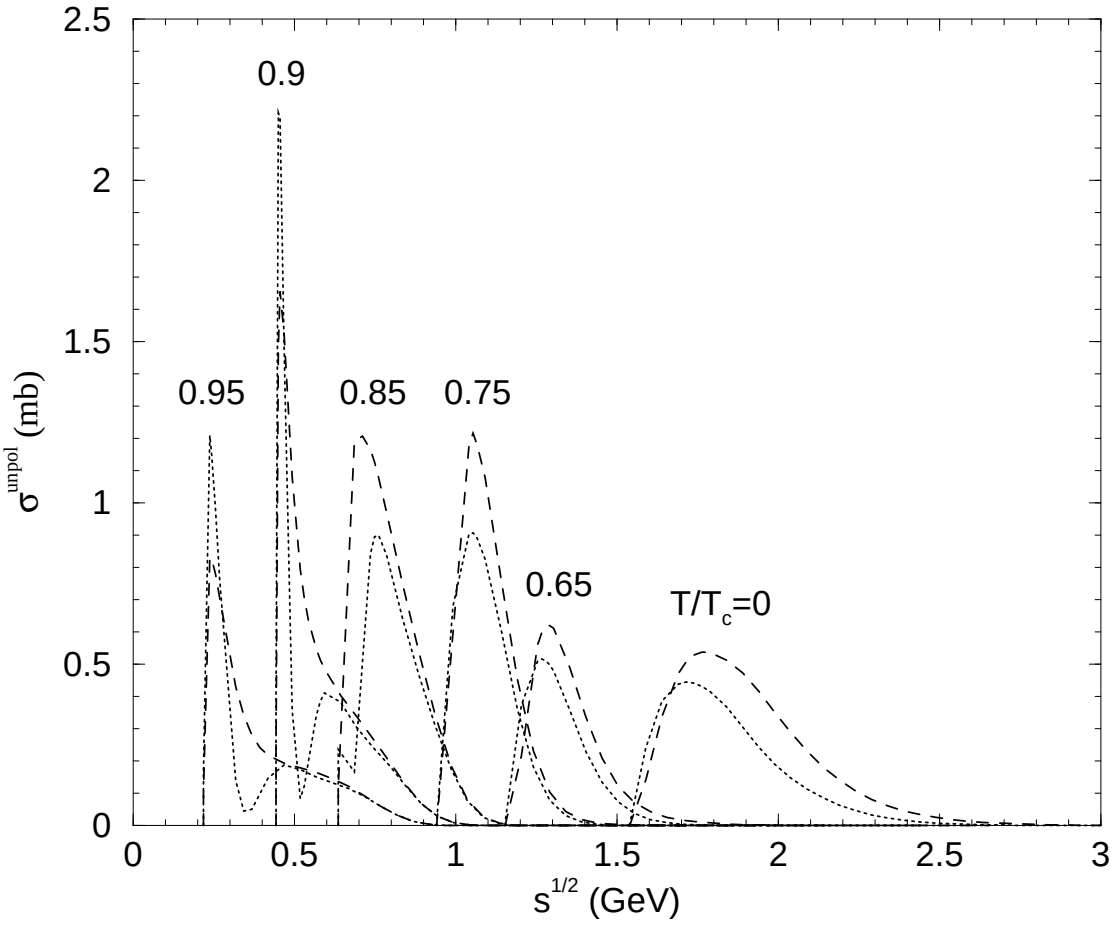

Figure 10: $\pi\pi \to \rho\rho$ cross sections for $I = 2$ in the prior form (dashed curves) and in the post form (dotted curves) at various temperatures.